**Atmospheric
Chemistry
and Physics**

Seasonal cycles and variability of O_3 and H_2O in the UT/LMS during SPURT

M. Krebsbach[1], **C. Schiller**[1], **D. Brunner**[2], **G. Günther**[1], **M. I. Hegglin**[2], **D. Mottaghy**[3], **M. Riese**[1], **N. Spelten**[1], and **H. Wernli**[4]

[1]Institute for Chemistry and Dynamics of the Geosphere: Stratosphere, Research Centre Jülich GmbH, Jülich, Germany
[2]Institute for Atmospheric and Climate Science, Federal Institute of Technology, Zurich, Switzerland
[3]Applied Geophysics, RWTH Aachen University, Aachen, Germany
[4]Institute for Atmospheric Physics, University of Mainz, Mainz, Germany

Abstract. Airborne high resolution in situ measurements of a large set of trace gases including ozone (O_3) and total water (H_2O) in the upper troposphere and the lowermost stratosphere (UT/LMS) have been performed above Europe within the SPURT project. SPURT provides an extensive data coverage of the UT/LMS in each season within the time period between November 2001 and July 2003.

In the LMS a distinct spring maximum and autumn minimum is observed in O_3, whereas its annual cycle in the UT is shifted by 2–3 months later towards the end of the year. The more variable H_2O measurements reveal a maximum during summer and a minimum during autumn/winter with no phase shift between the two atmospheric compartments.

For a comprehensive insight into trace gas composition and variability in the UT/LMS several statistical methods are applied using chemical, thermal and dynamical vertical coordinates. In particular, 2-dimensional probability distribution functions serve as a tool to transform localised aircraft data to a more comprehensive view of the probed atmospheric region. It appears that both trace gases, O_3 and H_2O, reveal the most compact arrangement and are best correlated in the view of potential vorticity (PV) and distance to the local tropopause, indicating an advanced mixing state on these surfaces. Thus, strong gradients of PV seem to act as a transport barrier both in the vertical and the horizontal direction. The alignment of trace gas isopleths reflects the existence of a year-round extra-tropical tropopause transition layer. The SPURT measurements reveal that this layer is mainly affected by stratospheric air during winter/spring and by tropospheric air during autumn/summer.

Normalised mixing entropy values for O_3 and H_2O in the LMS appear to be maximal during spring and summer, respectively, indicating highest variability of these trace gases during the respective seasons.

1 Introduction

Ozone and water vapour are important absorbers of solar irradiance and emitters/absorbers of terrestrial radiation. Both species have direct and indirect effects on radiative forcing and/or photolysis rates and therefore play a decisive role for the radiative budget of several atmospheric regions, for chemistry and climate. They are further suitable trace gases to investigate and understand transport and mixing processes, especially in the region of the upper troposphere and lowermost stratosphere (UT/LMS). This part of the atmosphere is to a large extent affected by dynamics, and in particular by bi-directional stratosphere-troposphere exchange. Trace gas distributions in the UT/LMS depend strongly on the interaction between dynamical and chemical processes near the tropopause. Changes in the chemical composition of the UT/LMS have a strong impact on atmospheric radiation. A detailed understanding of the trace gas distributions, their variability, underlying processes and transport mechanisms of natural and anthropogenic emissions is crucial for climate prediction and radiative feedback mechanisms, in particular, when considering global warming scenarios (e.g. Lindzen, 1990; Rind et al., 1991; Inamdar and Ramanathan, 1998) and in climate simulations (e.g. McLinden et al., 2000). The UT/LMS and especially the tropopause region is thus of significant scientific interest.

Correspondence to: M. Krebsbach
(m.krebsbach@fz-juelich.de)

Several data sets of satellite instruments have been analysed to infer seasonal distributions of ozone and water vapour in the LMS as well as connected transport mechanisms. From SAGE II measurements, Pan et al. (1997) inferred ozone and water vapour distributions in the LMS and compared them to MLS and ER-2 measurements (Pan et al., 2000). MLS water vapour data was further investigated by Stone et al. (2000) regarding climatological aspects as well as spatial and temporal variability. Randel et al. (2001) and Park et al. (2004) used HALOE data to derive seasonal variation of water vapour in the LMS. Furthermore, ozone and water vapour data in the UT and LMS from POAM III measurements were analysed by Prados et al. (2003) and Nedoluha et al. (2002), respectively. Satellite observations are thus a powerful tool for a global data coverage of the whole atmosphere. Nevertheless, there are several disadvantages and restrictions given by nature and technology, in particular, the limited spatial resolution. Due to the restrictions and the lack of satellite data in the UT/LMS, the tropopause region is rather under-sampled. Highly accurate and resolved observations of the UT/LMS can only be achieved with in situ measurements. For instance, Strahan (1999) analysed ozone data from ER-2 flights in the potential temperature region between 360 K and 530 K. Aircraft measurements are commonly quite sporadically distributed in time and space. For such purposes, projects like MOZAIC (e.g. Marenco et al., 1998), NOXAR (e.g. Brunner et al., 1998) or CARIBIC (e.g. Brennikmeijer et al., 2005) use commercial and passenger aircraft to routinely measure chemical species, but thereby only the lower part of the LMS is reached.

Within the very successful aircraft project SPURT (German: SPURenstofftransport in der Tropopausenregion, trace gas transport in the tropopause region) in the European sector (30° E to 30° W, 30° N to 80° N) an extensive high quality data coverage of the UT/LMS in each season was obtained. Using a Learjet 35A a total of eight campaigns, evenly distributed in time between November 2001 and July 2003, were performed, resulting in a total number of 36 flights of on average 4 h duration. Each season (autumn, winter, spring, and summer, corresponding to the months SON, DJF, MAM, and JJA) was investigated with two campaigns. Depending on meteorological conditions, the aircraft's ceiling altitude is about 14 km and thus allows for sampling in the LMS during all seasons, even at subtropical latitudes. The SPURT measurements between the 280 K and 380 K isentropes thus contribute significantly to the data coverage in the whole extra-tropical LMS above Europe. A description of the project strategy, its aims, performance and instrumentation is given in an overview paper by Engel et al. (2005).

The purpose of this work is to analyse the seasonality and variability of ozone (O_3) and total water (H_2O) in the UT/LMS as measured during the SPURT project. After a short description of these trace gas measurements, the seasonal cycles of O_3 and H_2O are discussed. Several statistical perspectives are used to investigate trace gas variability and

implications for the trace gas distribution in the probed atmospheric region.

2 The SPURT O_3 and H_2O data

During the SPURT campaigns, O_3 was measured with UV absorption by the JOE instrument (Jülich Ozone Experiment, Mottaghy, 2001). For most flights, i.e. from the third campaign on, O_3 was additionally measured by a chemiluminescence detector ECO-Physics CLD 790-SR (Hegglin, 2004). Inter-comparison of both instruments results in high consistency with a 6.4% difference which is in the uncertainty range of both instruments (Hegglin, 2004; Engel et al., 2005). However, in the presented analyses here the JOE data is preferably considered and ECO data are only used if no JOE data are available. Total water, i.e. the sum of vapour and vaporised ice, was measured with the photofragment-fluorescence technique by the FISH instrument (Fast In situ Stratospheric Hygrometer, Zöger et al., 1999). The instruments JOE, ECO and FISH have a time resolution of 10, 1, 1 s, and an accuracy of 5, 5, 6%, respectively. Due to the different integration times of the single instruments the measurement data was analysed as 5 s data. Thereby, the JOE data was interpolated to the centre interval, measurements with a higher sampling rate were averaged over each 5 s. For an average aircraft flight speed of 150 to 200 m s^{-1} this results in a mean spatial resolution of 0.75 to 1.00 km. For a complete listing of the Learjet payload, data availability, and for details about the processing of the whole SPURT data set see Engel et al. (2005).

Figure 1 gives an impression of the obtained coverage of O_3 (and H_2O) measurements during SPURT in the geographical and potential temperature space. The map in the left panel reflects the number of measurements in a 1° longitude×1° latitude bin. Each campaign consisted of a minimum of 2 flight days. On one day southbound and on the other day northbound flights were performed from and back to the Learjet basis Hohn (9.53° E, 54.31° N, northern Germany). The contours clearly accentuate the basis in northern Germany as well as the two main inter-stations, Faro in southern Portugal for the southbound flights and Tromsø in Norway for the northbound flights. Slow ascents and descents in these regions result in a large number of measurements there.

The right panel of Fig. 1 shows seasonal frequency distributions of data points in potential temperature intervals from 280 K to 380 K in steps of 10 K. Potential temperature (Θ) is calculated from avionic measurements of pressure (p) and temperature (T), the latter two having an uncertainty range of ±1 hPa and ±0.5 K, respectively. The distributions indicate winter and spring with more than 23 000 and 25 000 data points, respectively, as the best captured seasons. With more than 19 000 data points also the autumn and summer season are probed quite well. The tail at the lower Θ values between
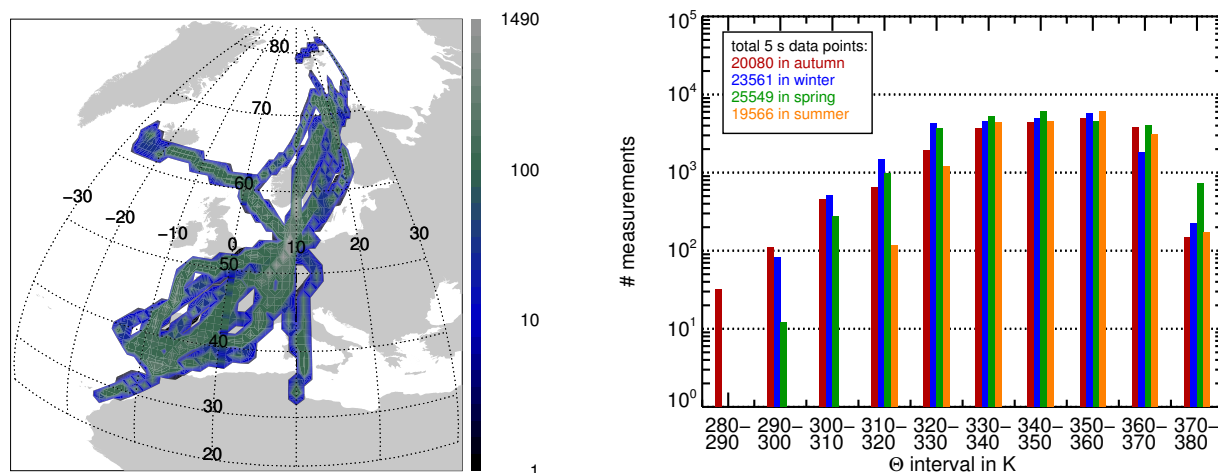
Fig. 1. Distributions of obtained O_3 measurements during SPURT. Approximately the same distribution is valid for H_2O (cf. Table A1 in the Appendix). In the map (left), the number of 5 s data points in a $1°$longitude $\times 1°$ latitude grid is displayed. The colour bar reflects the number of data points in each geographical bin. The right chart shows frequency distributions of the same data in the potential temperature space, binned in 10 K steps. By this approach, a seasonal separation is performed (autumn, winter, spring, and summer, corresponding to red, blue, green, and orange, respectively). The total number of merged data points within the considered Θ range in each season is given in the upper left corner.

280 K and 310 K is a result of sampling, since the inlet of the FISH instrument was only opened at altitudes higher than a pressure value of ≈ 400 hPa. Similarly, the JOE instrument provides high qualitative data at pressure altitudes above that pressure level (i.e. $p < 400$ hPa). The frequency distributions in the Θ space reflect the SPURT concept of the flight profiles. Slow ascents and descents allowed for accurately resolved slant vertical profiles. Within each mission two flight legs at rather constant pressure altitude were performed, one near and the other above the tropopause (cf. numbers of data points within 320 K and 340 K and 350 K and 370 K, respectively). Due to fuel consumption and thus lower mass of the aircraft, at the end of each mission a climb to maximum altitude (>370 K) was performed to sample generally undisturbed stratospheric background air. The altitude flight profile was mirrored on the return flight to Hohn to sample the meteorological condition in two different height regimes.

To place the measurements in a meteorological context, ECMWF (European Centre for Medium-Range Weather Forecasts) analyses with a time resolution of 6 h interpolated to a $1° \times 1°$ grid in longitude and latitude on 21 pressure levels between 1000 and 1 hPa are used. Each analysis data set was further interpolated to 25 isentropic surfaces located between 280 K and 400 K in steps of 5 K. On these isentropes potential vorticity (PV) is obtained by spatial and temporal interpolation to the flight tracks. The diagnosis of PV from meteorological data fields is affected by errors (e.g. Beekmann et al., 1994; Good and Pyle, 2004). The procedure of data assimilation will remove obvious observational errors (Hollingsworth and Lönneberg, 1989). The accuracy

in calculating PV is sensitive to the horizontal and vertical resolution and, in particular, small-scale meteorological features like tropopause folds are hardly represented in detail in the meteorological analyses. In contrast, in situ measurements have a much finer resolution and can therefore resolve small-scale features. This has to be considered when correlating model derived quantities with in situ measurements (cf. Sect. 4).

3 Seasonal cycles of O_3 and H_2O in the UT and LMS

In order to derive seasonal cycles of O_3 and H_2O in the UT and LMS, PV is used to categorise air parcels. Since PV increases with height and latitude in the northern hemisphere, it is used here to split the data set into atmospheric subsets. Detailed analyses of vertical profiles during ascents and descents reveal a PV value of 2.0 to 2.5 PVU (1 PVU=10^{-6} m^2 s^{-1} K kg^{-1}, according to Hoskins et al., 1985) as representative for the location of the extra-tropical tropopause during SPURT (e.g. Hoor et al., 2004, Krebsbach, 2005, Hegglin et al., 2005). Potential vorticity values lower than 1 PVU are therefore assumed to denote air measured in the upper troposphere (restricted to pressure altitudes above ≈ 400 hPa), values within the range 1–3 PVU data observed in the tropopause region, and higher PV values reflect an increasing stratospheric character of the probed air.
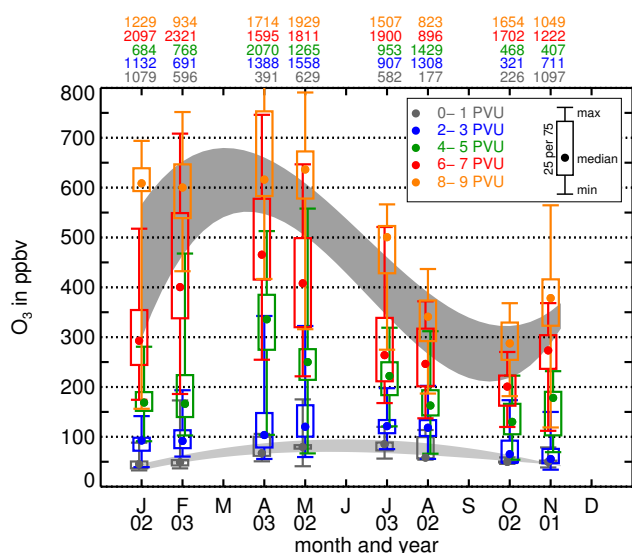
Fig. 2. Annual cycles of ozone mixing ratios in ppbv in the region of the UT and LMS as derived from the SPURT measurements. The observations are displayed as box plots in terms of potential vorticity, non-continuously incremented by 1 PVU due to facility of inspection (colour coding for 0–1, 2–3, 4–5, 6–7, 8–9 PVU), as indicated in the upper right corner. The median in each PV interval is represented by a dot, the box reflects the 25 and 75 percentiles, and the whiskers indicate minimum and maximum O_3 VMRs. Note the month-year relation given by the labelling of the abscissa. The number of data points considered in each box plot is given colour coded in the top row. The light and dark grey shadings display 3rd order polynomials fitted to the quartiles of O_3 data in the 0–1 PVU and 7–9 PVU range, to approximate the tropospheric and stratospheric seasonal cycles of O_3 as observed during SPURT, respectively.

3.1 O_3 in the UT and LMS

In Fig. 2 monthly median O_3 volume mixing ratios (VMRs) in different PV domains, characteristic for specific regions of the atmosphere, are shown as measured during SPURT. Thereby, a box plot graphing is used, showing centring (median), spread (25 and 75 quartiles), and distribution (minimum and maximum). Despite the high information content presented by the box plots, they can lead to misinterpretation or over-valuation of attributes in case of insufficient data. To provide an accurate impression of the central tendency and variability of O_3 the number of considered data points in each box plot is additionally given in the top row, revealing that the considered amount of data in a PV domain should mainly be large enough to infer robust information from the box plots. Considering the complete data set, the seasonal variation of O_3 in the UT shows a minimum during the winter and a broad maximum during the spring and summer measurements. This is highlighted by the light grey shading, representing 3rd order polynomial fits to the quartiles of O_3 measurements in the 0–1 PVU range.

There exists a number of regions showing a broad summer maximum in tropospheric ozone. The existence of such a maximum is often associated with photochemical production (e.g. Logan, 1985). Thereby, O_3 is formed by reactions involving volatile organic compounds and nitrogen oxide (NO_x), driven by solar radiation. Many of these regions are continental and influenced by pollution (e.g. Logan, 1989; Scheel et al., 1997). Also in the free troposphere, a broad spring to summer maximum was observed (e.g. Logan, 1985; Schmitt and Volz-Thomas, 1997). Based on ozone sonde data from Observatoire de Haute-Provence (OHP) Beekmann et al. (1994) showed that the seasonal variation of tropospheric O_3 is characterised by a large maximum during spring and summer. Furthermore, LIDAR and ozone sonde measurements from OHP from 1976 to 1995 give evidence for a shift from a spring maximum to a spring/summer maximum in the free troposphere (Ancellet and Beekmann, 1997). The observed broad spring/summer O_3 maximum during SPURT in the UT with a slight shift towards spring is furthermore in accordance with results from Brunner et al. (2001).

Most variable O_3 VMRs were observed during the spring campaigns. During this season the influence of the large-scale downward motion is most prominent (Appenzeller et al., 1996). Also the net O_3 flux across the extra-tropical tropopause has a peak during spring to early summer, primarily affected by the outward O_3 flux of the LMS through the tropopause (Logan, 1999). Thus, the already enhanced tropospheric O_3 VMRs during spring seem to be effected by the downward transport of O_3-rich stratospheric air during that season.

Measurements at Mace Head, Ireland, illustrate a clear spring O_3 maximum (Derwent et al., 1998). However, the appearance of a spring maximum in the O_3 seasonal cycle in the northern hemisphere troposphere is heavily debated (cf. review by Monks, 2000). Regarding northbound and southbound flights during SPURT separately (not shown here), the maximum in tropospheric O_3 VMRs were observed in late spring (May 2002) for higher latitudes and in summer (July 2003) further south (cf. Krebsbach, 2005). This is in agreement with results of Scheel et al. (1997) from low-altitude and mountain sites between 28–79° N. Further, Hough (1991) showed by 2-dimensional model studies the general maximum of O_3 precursors like NO_x, carbon monoxide, and hydrocarbons in the free troposphere at middle and higher latitudes during winter and spring, which is in accordance with the slight shift towards spring observed during the northern SPURT flights. As mentioned before, a contribution to higher O_3 VMRs in the UT during spring is presumably affected by a contribution of O_3-rich air due to stratosphere-to-troposphere transport. The observed maximum in O_3 VMRs during summer is possibly a result of in situ photochemical production (e.g. Logan, 1985; Haynes and Shepherd, 2000) since photochemical activity is expected to be highest during this period (e.g. Liu et al., 1987).

In PV domains >3 PVU, in the LMS, a clear maximum during the spring and a minimum around the autumn measurements is evident with a peak-to-peak amplitude of ≈400 ppbv O_3 within the PV range of 8–9 PVU. The quartiles of O_3 measurements in the 7–9 PVU range are fitted by 3rd order polynomials, assigned by the dark grey shading, to highlight the seasonal cycle of O_3 measured in the LMS. The ozone build-up in this atmospheric region occurs during winter as a consequence of poleward and downward transport, since the lifetime of O_3 is long with respect to chemical loss (e.g. Holton et al., 1995) and is largely controlled by dynamics (Logan, 1999). The observed spring maximum in the LMS over Europe during SPURT is most probably due to the downward advection of high O_3 VMRs by the stratospheric winter/spring Brewer-Dobson circulation, in accordance with e.g. Logan (1985), Austin and Follows (1991), Oltmans and Levy II (1994), Haynes and Shepherd (2000), Prados et al. (2003). Ozone VMRs fall off from April/May to October with a strong average decrease rate in the 6–9 PVU range of ≈−78 ppbv/month. Much of this decrease is presumably caused by the change in tropopause height and transport mechanisms. On the basis of observations of SAGE II, Pan et al. (1997) and Wang et al. (1998) assumed that isentropic cross-tropopause inflow of tropospheric air into the LMS influences the seasonal cycle of O_3 (and H_2O, see Sect. 3.2) in that atmospheric region, especially during summer. A maximum of quasi-isentropic inflow into the LMS during summer was also identified in model studies by Chen (1995, 2-dimensional) and Eluszkiewicz (1996, 3-dimensional). Enhanced content of tropospheric air in September compared to May was identified by Ray et al. (1999) from balloon-borne chlorofluorocarbons and water vapour measurements, which was also thought to be owing to quasi-isentropic in-mixing of tropospheric air. The seasonal cycle of O_3 in the extra-tropics therefore differs between the UT and the LMS. The transition region between the UT and LMS (1–3 PVU) is rather influenced by the troposphere. Just above the tropopause layer (4–5 PVU) the stratospheric signal becomes dominant.

Amplitudes of O_3 VMRs grow with increasing PV. Regarding the progression of O_3 VMRs through surfaces of increasing PV, the most prominent increase is apparent during winter and spring, whereas during summer and autumn the gradients are comparably weak. Since in Fig. 2 rather dynamically similar air parcels are considered and PV exhibits a transport barrier, the lower O_3 gradients with respect to PV surfaces during summer and autumn suggest an intensified transport of tropospheric air into the LMS during these seasons (cf. Sect. 3.2). Towards higher PV ranges (>3 PVU), i.e. deeper in the LMS, tropospheric influence decreases which results in an increase in the slope (dO_3/dPV). The observed variation of the slope has a maximum of about 60–90 ppbv/PVU in April and a minimum of 10–30 ppbv/PVU in October. The results are comparable with findings from Beekmann et al. (1994) and Zahn et al. (2004).

3.2 H_2O in the UT and LMS

As ozone, water vapour shows a distinct vertical gradient at the extra-tropical tropopause. Due to the temperature lapse rate and the decrease in pressure, water vapour VMRs decrease exponentially with height from the troposphere up to the tropopause region. Calculated averages of measurements that span the transition region between the UT and the LMS are dominated by moist air from below the tropopause.

In Fig. 3 monthly values of H_2O measured during SPURT are depicted in the same manner as for O_3 (cf. Fig. 2). It is to note that the box plots in Figs. 2 and 3 are not displayed chronologically in time (see labelling of abscissas). Based on the annual cycle of tropopause temperatures (e.g. Hoinka, 1999) and resulting ice saturation VMRs, maximum H_2O VMRs in the tropopause region are expected during the summer, lowest during the winter months. In the PV range 0–1 PVU maximum H_2O VMRs were measured during the campaign in August 2002. Alongside, the spring campaign in April 2003 shows a second tropospheric maximum, whereas during May 2002 and July 2003 comparably low H_2O VMRs are apparent. This reflects the high variability of H_2O in the probed atmospheric region, but is likely also sensitive to sampling (opening and closure altitude of the FISH inlet during ascents and descents). A tendency of higher VMRs during summer and lower ones during winter is present, which is evident from the accordant box plots in the 1–2 PVU (not shown) and 2–3 PVU range. As in Fig. 2, 3rd order polynomials are fitted to the measurements in the 0–1 PVU range (light grey shading), to approximate the annual cycle of H_2O in the UT. Across the tropopause the strong gradients in H_2O are apparent. Considering northbound and southbound flights separately, the tropopause region at lower latitudes is slightly dryer than further north. This is probably due to the stronger influence of the dryer subtropical regions (see for instance Hoinka, 1999; Krebsbach, 2005).

In the LMS (>3 PVU) a clearer seasonal cycle in H_2O than in the UT can be deduced from the measurements, again with the maximum measured during August 2002. Unfortunately, on the northbound flights during this campaign, problems with the FISH instrument were encountered. Hence, H_2O data are only available for the southbound missions, leading to a reduced amount of data points above ≈6 PVU (see number of data points in top row). Again, the dark grey shading shows 3rd order polynomial fits to the quartiles in the 7–9 PVU range, to highlight the approximation for the observed annual cycle of H_2O in the LMS. As in the UT there is a tendency of highest H_2O VMRs during summer. This maximum is in agreement with previous in situ and remote observations (e.g. Mastenbrook and Oltmans, 1983; Foot, 1984; Oltmans and Hofmann, 1995; Dessler et al., 1995; Pan et al., 1997; Stone et al., 2000) but can not be stated with sufficient certainty from the SPURT data alone, as mentioned in the introduction.
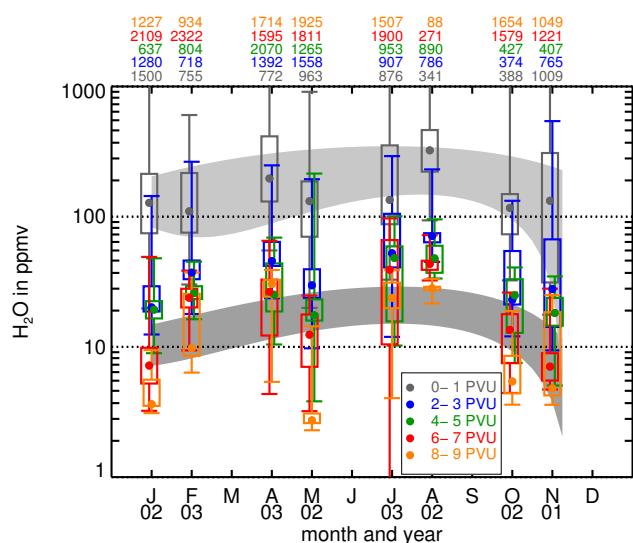
Fig. 3. As Fig. 2, but for total water mixing ratios (in ppmv).

The measurements in February and April 2003 show higher H_2O VMRs in the LMS than in May 2002, which probably indicates significant inter-annual variability but can also be influenced by sampling. The major part of flight legs during the southbound measurements in May 2002 were situated in the vicinity of the tropopause. The meso-scale dynamics indicates presence of subtropical air in the southern measurement region, i.e. lower in H_2O and O_3 compared to mid and high latitude air (e.g. Hoinka, 1999; Krebsbach, 2005). In contrast, the aircraft extends deep into the stratosphere on the northbound missions (cf. number of data in the 6–7 and 8–9 PVU ranges). This results in the established distribution of lower H_2O VMRs in May compared to April 2003 in the 4–7 PVU range and thus largely affects the course of the approximated polynomials near MAM.

Air in the so called "overworld" (Hoskins, 1991) is dehydrated as it is transported through the tropical cold trap. However, for a large extent of the performed SPURT campaigns H_2O VMRs are considerably enhanced compared to stratospheric background values of about 2–6 ppmv (e.g. Hintsa et al., 1994). In the upper considered PV bins (>7 PVU) median values of observed H_2O VMRs during the summer campaigns are about 20–30 ppmv and are moreover even measured in February and April 2003. These VMRs are much higher than could solely be explained by entry of air into the (lowermost) stratosphere in the tropics (e.g. Foot, 1984; Nedoluha et al., 2002). Values substantially larger than ≈ 6 ppmv are evidence for transport mechanisms of air into the LMS across the extra-tropical tropopause, and this signature is carried deep into the lower stratospheric region.

Although there is no indication for a measurement artifact, the enhanced H_2O VMRs observed in the LMS evoke consideration of instrument problems, e.g. cabin air leak, but which most likely can be excluded for several reasons. For instance, the campaign in February 2003 started with the

southbound flights where H_2O VMRs of 20–30 ppmv concomitant with 400–700 ppbv O_3 were measured. On the northbound flights on the next day, H_2O VMRs <6 ppmv were observed at O_3 VMRs of 600–750 ppbv, indicating that FISH was able to measure low stratospheric H_2O VMRs, in particular, no changes were performed on the FISH instrumentation during the whole campaign. The H_2O VMRs measured during spring 2003 are also enhanced at PV levels above ≈ 6 PVU. This campaign started on 27 April with the northbound flights where beside H_2O VMRs <7 ppmv exceptional enhanced H_2O VMRs of about 20–35 ppmv were observed at O_3 VMRs >600 ppbv. During the southbound flights, no such "abnormal" stratospheric conditions were encountered. Fortunately, an added flight for inter-comparison of NO_y instruments on the next day headed northward, allowing to measure once more in the region probed two days before. Again H_2O VMRs of 25 ppmv concomitant with O_3 VMRs >600 ppbv were measured, which provides evidence for the correctness of data and debilitate instrument problems with leakage. Moreover, the SPURT flight concept, where most of the outbound flight legs were mirrored on the return flights to the campaign base, albeit at different altitudes, allows to cross-check the sampling on these southbound and northbound flights. Thereby, the H_2O distributions are largely affirmed by both flights, suggesting robustness of the measured data.

Although enhanced H_2O VMRs in the LMS are exceptional, such conditions were encountered in all seasons during SPURT and thus seem not to be unlikely. Hegglin et al. (2004) discussed such an event probed during November 2001, and related it to the effect of recent convection with high reaching tropospheric injections during that time period. Also Tuck et al. (2003) reported about ER-2 flights near 60° N in February 1989 with similar observations. Comparable high amounts of H_2O accompanied with high O_3 VMRs were discussed recently by Dessler and Sherwood (2004) for the summer season and are also consistent with trace gas analyses by Ray et al. (2004b). Alongside, comparisons by Günther et al. (2004) of the SPURT observations with e.g. air mass spectra derived from model studies with the Chemical Lagrangian Model of the Stratosphere demonstrate good agreement.

Another possible explanation for the encountered enhanced H_2O VMRs is provided by trajectory calculations. These occasionally suggest that air during troposphere-to-stratosphere transport processes is not generally freeze-dried to its saturation value, by reason that e.g. the time for an effective sedimentation and thus removal of ice water is too short. Saturation is rare in the LMS, allowing H_2O-rich air to persist for a very long time period there. These aspects are currently investigated in more detail.

In contrast to O_3, with increasing PV the H_2O VMRs as well as the amplitude of the annual cycle decrease (note the logarithmic scale). This indicates a more pronounced seasonal cycle of H_2O in the LMS below ≈ 5 PVU.

Combining the measurements of both campaigns in each season, the seasonal variability of H$_2$O for observations in the tropopause region and in the LMS increases from SON/DJF towards JJA (see also Sect. 4). Note that the low variability of H$_2$O in the PV bins above 6 PVU for the campaign in August 2002 is affected by the reduced amount of data, as mentioned earlier. The increase in variability towards summer suggests that the potential for transport of water through the tropopause is more effective and thus more important and significant during this season. This is especially relevant for long-term transport which is the combined effect of mass transport and the efficiency of freeze-drying. Hence, as already derived from the O$_3$ data, the LMS seems to be more influenced by the troposphere during summer than during winter which is in agreement with the discussed seasonal variability of water vapour in the LMS by e.g. Pan et al. (2000).

Whereas the O$_3$ maximum measured in the UT is approximately in phase with the observed H$_2$O maximum, it occurs about 2–3 months later (earlier) in the year as the O$_3$ maximum (minimum) in the LMS. A similar time lag was found by Pan et al. (1997) and Prados et al. (2003). Due to the large debate, especially concerning the often observed spring O$_3$ maximum at some northern hemisphere stations, it is necessary to further investigate to what extent the correlation and/or anti-correlation of both trace gases could be attributed to dynamics or to chemistry. The seasonal cycles of O$_3$ and H$_2$O obtained during the SPURT campaigns underline the influence of two competing processes in the UT/LMS region: (i) subsidence of dry air from the overworld, which is primarily determined by the low tropical tropopause temperatures and transported by the large-scale Brewer-Dobson circulation (e.g. Holton et al., 1995), and (ii) direct transport of moist air of tropical, subtropical or mid-latitude origin across the extra-tropical tropopause (e.g. Dessler et al., 1995; Hintsa et al., 1998). Whereas much of the air in the LMS has probably been transported into the stratosphere by the former process, it is likely that local vertical transport processes play a much larger role in determining H$_2$O in the UT/LMS. As is apparent in Fig. 3, in contrast to the O$_3$ VMRs, the observed seasonal cycles of H$_2$O in the UT and LMS are roughly in phase with each other. This same seasonal course in both atmospheric compartments is a priori not clear, for instance due to integral effects. In particular, there is a strong decrease in H$_2$O from August (maximum) where only measurements on southbound flights between 33–54° N are available, to October 2002. During August–October, the monsoons probably enrich the LMS with tropospheric air. This air could be dryer than air transported into the LMS at mid-latitudes during summer and would thus lead to a relative strong decrease of H$_2$O in the mid-latitude LMS. The observed lower H$_2$O VMRs in October 2002 (and November 2001) thus suggests a significant contribution of upper tropospheric (sub)tropical air which previously has entered the LMS (cf. also results of Hoor et al., 2005; Hegglin et al., 2005).

## 4 O$_3$ and H$_2$O in a view from different coordinates

The SPURT measurements covered a broad latitude range with different meteorological situations, often associated with small-scale phenomena (e.g. tropopause folds) and large-scale meridional advection of polar and/or subtropical and/or tropical air. The different dynamical impacts result in discontinuities and changes in the tropopause height, particularly in the vicinity of regions with high wind velocities, the jet streams, in the literature often referred to as the region of the "tropopause break". In order to get a comprehensive insight into distribution, spread, range, and variability of the measured trace gases in the SPURT region, 2-dimensional probability distribution functions (PDFs) are determined by using chemical, thermal, and dynamical vertical coordinates. Moreover, it is interesting to investigate which coordinate is best correlated with a trace gas and where the most compact correlation appears. An accurate correlation helps to deduce and to assess transport processes and provides the possibility for transformation into related quantities (see e.g. Krebsbach et al., 2006[1]).

4.1 Probability distribution functions

In several SPURT flights, distinct cross-tropopause exchange events and characteristic features for specific meteorological situations could be identified. To obtain a compact view of the probed atmospheric region, PDFs are a tool to centralise the large number of measurements. As an advantage of the PDFs, all measurement data is considered, and averaging is minimised. Thus, outliers become more visible and the prominent structures and features are revealed (Ray et al., 2004a).

In Fig. 4, PDFs of O$_3$ (left) and H$_2$O (right) as a function of the thermal vertical coordinate potential temperature for the spring season are depicted. For the distributions obtained for the other seasons it is referred to Krebsbach (2005). Ozone is binned by 20 ppbv, H$_2$O by 2 ppmv, and potential temperature by 5 K. The trace gas distributions are normalised to every bin of the thermal coordinate. This means, the colour coding reflects the probability in percent to measure a certain trace gas VMR at a certain potential temperature. In addition, the mean and median value in each Θ bin is represented by the solid and dashed coloured line, respectively. While the mean is an appropriate measure of the central tendency for roughly symmetric distributions, it is misleading when applied to skewed distributions since it can greatly be influenced by extremes. In contrast, the median is less sensitive to outliers and may be more informative and representative for skewed distributions. All seasonal means and medians are displayed to compare to each other (red, blue,

---

[1]Krebsbach, M., Schiller, C., Spelten, N., and Günther, G.: Characteristics of the extra-tropical transition layer as derived from O$_3$ and H$_2$O measurements in the UT/LMS during SPURT, in preparation, 2006.
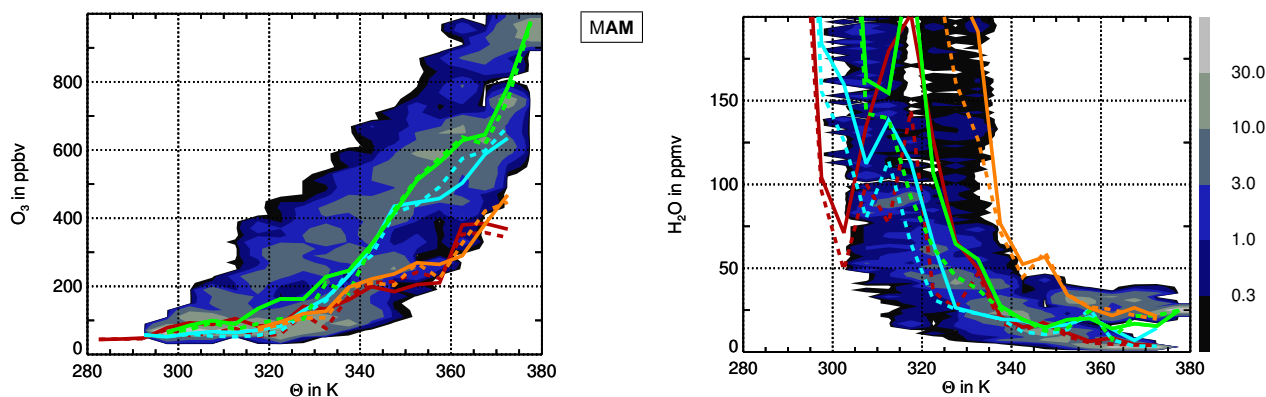
Fig. 4. Seasonal 2-dimensional probability distribution functions of O$_3$ (left) and H$_2$O (right) as a function of the thermal coordinate Θ for the spring measurements. The bin size is 20 ppbv for O$_3$, 2 ppmv for H$_2$O, and 5 K for Θ. The normalisation is performed to each Θ bin, i.e. the probability (colour coding) reflects the percentage of an observed trace gas VMR in a single Θ interval. In both panels the mean and the median trace gas mixing ratios in each Θ interval are given by the solid and dashed lines, respectively, and are seasonally compared to each other (red, blue, green, orange corresponding to autumn, winter, spring, summer). In addition, the amount of seasonal data points considered in each Θ bin are presented in Table A1.

green, and orange for autumn, winter, spring, and summer, respectively). From a statistical perspective it is desirable to acquire as much information as possible. The chosen bin sizes of trace gases and the reference coordinate result from sensitivity studies of bin widths, in order to resolve specific characteristics and to reduce smoothing while considering an accurate amount of data in each grid box. The sensitivity studies were performed for each reference coordinate considered in the following discussion. The seasonal number of data points in each Θ interval is displayed in Table A1 in the Appendix.

High probabilities, reflected by the light grey/green shadings, are very scattered throughout the O$_3$ distribution and, although both parameters, Θ and O$_3$, can be considered as vertical coordinates, no clear correlation is apparent. There is no symmetry around the mean or median values and multiple modes can be noted. Generally, an increase of O$_3$ VMRs with increasing Θ (height) is present, but the spread of O$_3$ VMRs on levels with constant potential temperature, the isentropes, is considerably large. The remarkable scatter and spread in the O$_3$ distributions is expected, since O$_3$ VMRs are largely dependent upon the location of the tropopause. The single flight missions extended over a large latitude range. Therefore, the variability of potential temperature at the tropopause location during each deployment along the flight path was sometimes quite large. For instance, on a flight from Hohn to Tromsø on 17 May 2002, the thermal tropopause (determined according to the WMO definition, WMO, 1986) was located at 304 K in the vicinity of Tromsø and at 328 K near the campaign base Hohn, which is a variation of 24 K (see Krebsbach, 2005). However, also at higher isentropes, i.e. further away from the local tropopause, the spread in O$_3$ VMRs is considerably high.

The H$_2$O PDF shown here as well as the distributions for the other seasons (see Krebsbach, 2005) exhibit similar characteristics as those for O$_3$. The large variation of the tropopause location is apparent in the high amounts of H$_2$O VMRs below $\approx$340 K, with several local maxima and minima in the course of means (and partly of the medians) between 300 and 320 K. A more compact distribution is only apparent above $\approx$340 K, with the higher variability during the summer season. Considering the largest seasonal differences of means and medians, i.e. between summer and winter, and shifting the mean H$_2$O VMRs above $\approx$330 K for the summer PDF by $\approx$20 K towards lower isentropes, the shape of the mean line (orange) is quite similar to the mean line for the winter season (blue). As illustrated by the number of considered data points in Table A1, the SPURT measurements are mainly concentrated in the atmospheric region above isentropes of $\approx$330 K. Strongest tropospheric influence during summer, as already mentioned in the previous section, is thus in agreement with the seasonally integrated mass flux through troposphere-to-stratosphere transport by Sprenger and Wernli (2003, their Fig. 3b).

The shapes of the O$_3$ PDFs for the winter and spring measurements are quite different from the distributions obtained for summer and autumn (see Krebsbach, 2005). Whereas the former distributions show a more compact shape with a steady rise in O$_3$ VMRs with increasing Θ, the latter are less compact with a relatively weak and partly even no increase in O$_3$ VMRs towards higher isentropes. This indicates an enhanced amount of air of recent tropospheric origin in the LMS compared to winter and spring. The large variability of trace gas VMRs, especially at higher isentropes (e.g. >400 ppbv O$_3$ at 360 K during all seasons) and the occurrence of several high probabilities on single isentropes, indicate that quasi-isentropic mixing is rather weak in this region.

The picture drawn on the basis of Θ changes significantly when shifting the thermal coordinate to a dynamic coordinate, namely PV. The corresponding trace gas PDFs are shown for all seasons in Fig. 5 with PV incremented in 0.5 PVU steps. As is directly evident, O_3 is much stronger correlated with PV than with Θ, which is rather an accurate height or correlation parameter in the undisturbed stratosphere. The range of O_3 VMRs on surfaces of PV is considerably suppressed when compared to the spread on isentropes and a general increase of O_3 with typically increasing height (PV) is now even apparent in the autumn and summer distributions. The highest probabilities are mostly centred in the distributions and symmetrically arranged around the mean or median O_3 VMRs. In the PDFs, the slopes of the trace gas versus PV are calculated (see top numbers in Fig. 5). Hereby, a linear fit was performed within 2 PVU intervals to point out the essential character. The slopes are significantly stronger within 2–4 PVU than within the 0–2 PVU interval. The means and medians show commonly a change in increase in this range, indicating 2 PVU as a good proxy for the dynamically defined extra-tropical tropopause during the SPURT missions. Of course, the slope is weaker during summer, owing to the annual cycle of O_3 in the UT and in the LMS. The distinct seasonal cycles of O_3 in both atmospheric compartments, the UT and LMS, are clearly apparent in the PDFs.

For H_2O, the spread in the PDFs is also reduced with PV as the reference coordinate. The sharp local minima and maxima in the mean and median values in the Θ space (cf. Fig. 4 between 300 and 320 K), which are due to the varying location of the local tropopause, are significantly reduced or even absent when related to PV. Also above 2–3 PVU, i.e. within the tropopause region, the variation of H_2O VMRs on PV surfaces is significantly reduced. However, during summer the H_2O derived distribution appears to be more compact when related to Θ. As is apparent from the structure as well as from the mean and medians, the seasonal cycles of H_2O in the UT and LMS are reflected in the PDFs, with certainly higher VMRs measured during the summer campaigns in the UT and in the LMS.

The trace gas VMRs show a more compact distribution in a dynamical sense. In contrast to the spread and distribution of several high probabilities on isentropic surfaces, Fig. 5 reveals that trace gas VMRs are more uniformly distributed and the probabilities vary less on PV surfaces. This indicates a more pronounced mixing state of trace gases on these surfaces rather than on isentropic surfaces.

A further coordinate system to look at the trace gas distributions and their variability is a coordinate system centred at the tropopause. Unfortunately, there was no instrument aboard the Learjet 35A measuring temperature profiles continuously along the flight track from which the tropopause altitude could be determined after the WMO definition (WMO, 1986). Nonetheless, as demonstrated earlier, the extra-

tropical tropopause during SPURT can be derived dynamically from a PV threshold value, i.e. 2 PVU. The actual distance in K of the aircraft's location to the local dynamical tropopause (denoted as $\triangle\Theta$) is derived from the afore described ECMWF analyses by taking a certain PV surface as the extra-tropical tropopause. Note, the data resulting from processing of the ECMWF analyses (e.g. PV, $\triangle\Theta$) are not identical to the data presented in Hoor et al. (2004), where higher resolved T511L60 ECMWF data were used. Intercomparisons for each campaign provide evidence for a clear agreement with correlation coefficients of >0.98 and slopes of 0.995 ($\pm$0.018). To account for the strong gradient of PV in the tropopause region, several PV threshold values were chosen as the dynamical extra-tropical tropopause, ranging from 2 to 6 PVU in 0.5 PVU steps. Through the different threshold values the character of the PDFs, i.e. location of high probabilities, spread and trace gas variability, does not change seriously. Thus, for representativeness, the O_3 and H_2O distribution related to the distance to the 2 PVU surface ($\triangle\Theta_2$) for the SPURT measurements during spring are shown in Fig. 6. For the distributions obtained during the other seasons as well as with $\triangle\Theta_4$ as the reference coordinate it is referred to Krebsbach (2005).

The PDFs with respect to the distance to a threshold value of PV and the course of means and medians highlight the strong change in trace gas composition near 2 PVU. The distributions are similar to those obtained in the PV space, albeit the use of $\triangle\Theta$ exhibits a slightly more compact shape, in particular for the campaigns in the winter and spring months (see also Sect. 4.3). The fact that the PDFs resemble in shape and distribution of probabilities in the view of PV and $\triangle\Theta$ suggests an advanced mixing state of these trace gases on surfaces aligned to the local tropopause. Each air parcel in the atmosphere can be thought of as being labelled by its PV, controlling or restraining the air parcels' range of motion. A relatively huge degree of freedom is given in regions of uniform PV (Sparling and Schoeberl, 1995). Thus, spatial gradients of PV might account for the dynamical affected trace gas distributions and not solely its absolute values. And this is exactly what the PDFs for different PV threshold values for the dynamically defined extra-tropical tropopause show, since the shape and the spread of distributions remain to the largest extent the same. This implies that the extra-tropical transition layer follows surfaces of PV or surfaces relative to the shape of the local tropopause, if defined by PV, rather than isentropic surfaces, in consistence with the results of Hoor et al. (2004).

4.2 Mixing entropy

A useful measure for the quality of correlation and variability of a trace gas in the PDFs is the mixing entropy, which could in general be regarded as a measure for uncertainty. For a uni-modal PDF the characterisation is reliably given by the first and second moments, e.g. mean and variance,
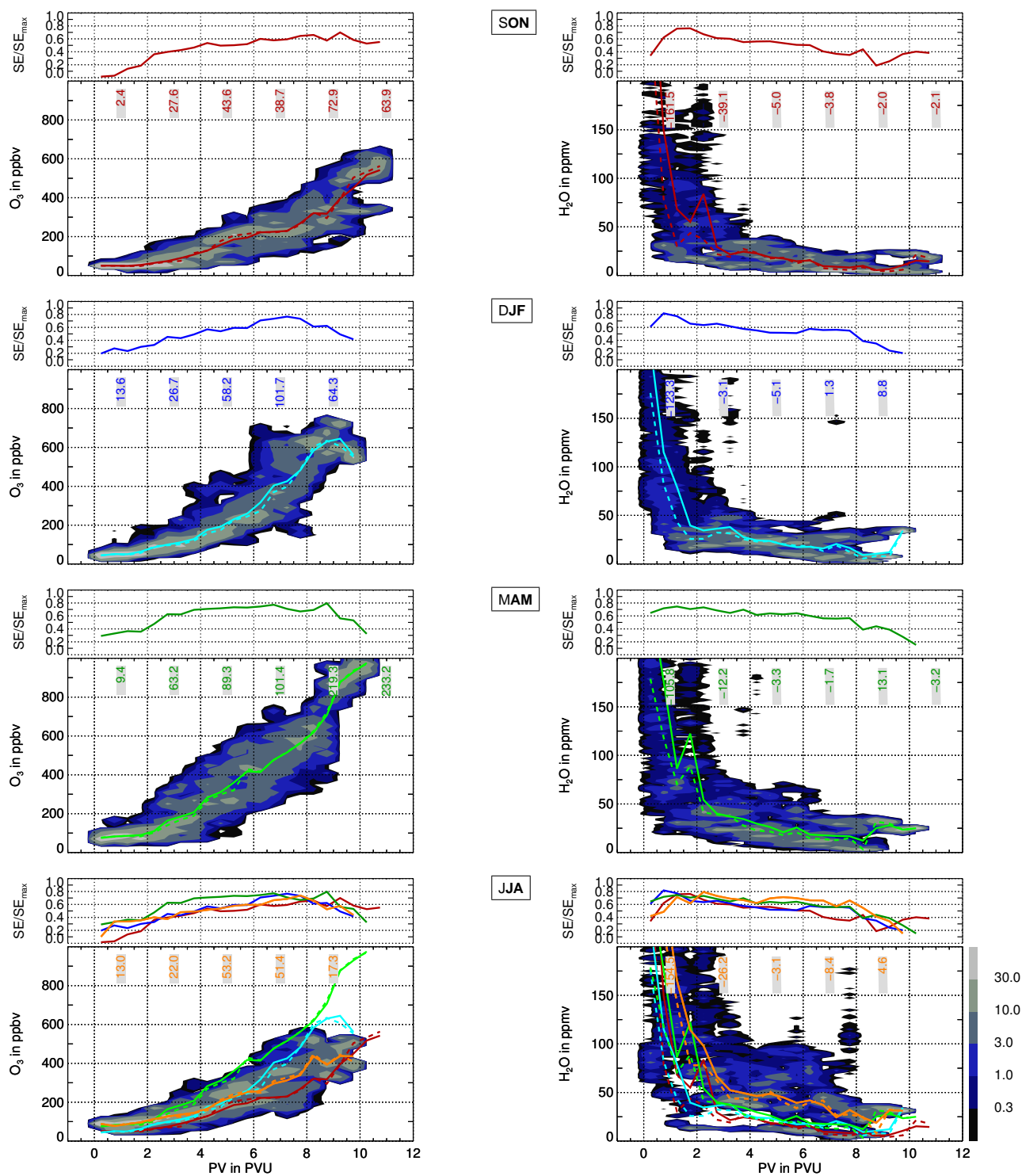
Fig. 5. As Fig. 4, but for all seasons and as a function of the dynamical coordinate PV. The bin size for PV is set to 0.5 PVU. In the top panels of the PDFs the normalised mixing entropy in each PV bin is displayed (see Sect. 4.2), also seasonally compared in the bottom charts. As a numeric value for the trace gas change with PV, the slope of a linear fit of data points, calculated in a 2 PVU bin width (unit [trace gas]/[reference coordinate]) is reflected by the numbers in the PDFs. From top to bottom: autumn, winter, spring, and summer. The amount of considered data points in each PV bin are presented seasonally separated in Table A2.
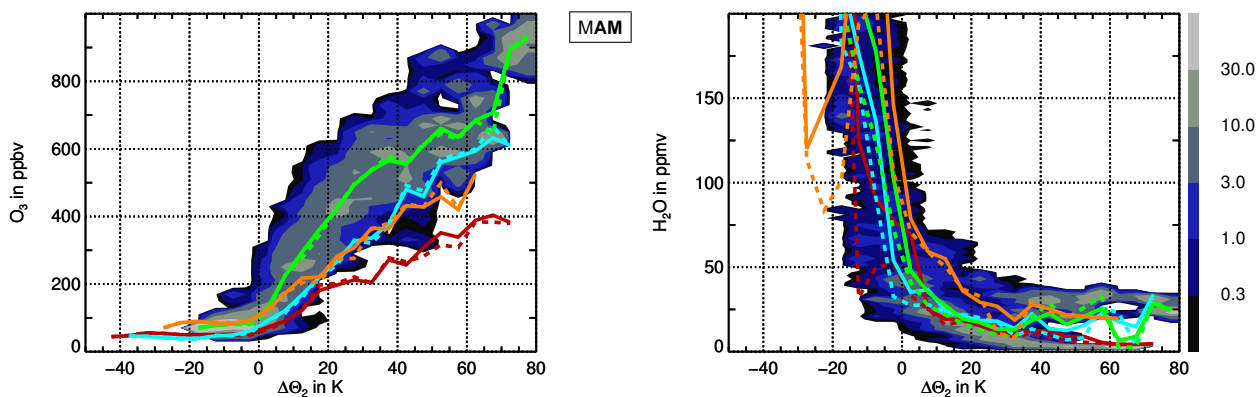
Fig. 6. As Fig. 4, but related to the distance to the local tropopause in K, considered as the 2 PVU surface. The bin size for $\triangle\Theta_2$ is 5 K, the number of considered data points in each $\triangle\Theta_2$ bin is given in Table A3.

respectively. Using these moments, the PDF is described by a relation to a single reference value, like the mean. This is probably inaccurate for a multi-modal distribution, where there is no symmetry around the reference (Sparling, 2000). A measure for the information content in a PDF for a trace gas μ provides Shannon's entropy which is given as

$$SE = -\sum_{i=1}^{N} p_i \cdot \ln p_i \qquad (1)$$

(e.g. Srikanth et al., 2000), with ln as the natural logarithm. Concerning a PDF with D total observed data points of trace gas μ and N bins of width $\triangle\mu$, the fraction of observation in the ith cell (p_i) is the number of observations within this cell (N_i) divided by D, and $\sum_{i=1}^{N} p_i = 1$. The information content is therefore solely dependent upon a given probability distribution and does not directly relate to the content or meaning of the underlying events, i.e. the quantity of the binned trace gas. Only the probability of the occurring events is important, not the events themselves. SE is zero if the distribution has a maximum concentration, e.g. chemical homogeneity within one bin. For a uniform spatial distribution, i.e. $p_i = 1/N \ \forall i$, the considered trace gas field has a maximum variability (any observed value can be placed in any one of the N bins) and the entropy is maximal ($SE = SE_{\max} = \ln N$). A maximum entropy implies indistinguishability of the air parcels. Moreover, they have an unrestricted free range of motion. In reality, PV constrains the air parcels' range of motion. Thus, a maximum entropy value is not to be expected (Sparling and Schoeberl, 1995). The maximum entropy is dependent upon the number of bins (see comment in Sect. 4.1). For a better comparison of different entropy values, a normalisation to the maximum entropy is performed, resulting in

$$\frac{SE}{SE_{\max}} = -\sum_{i=1}^{N} p_i \cdot \log_N p_i \leq 1 . \qquad (2)$$

The normalised mixing entropy is illustrated for O$_3$ and H$_2$O with PV as the reference coordinate above each seasonal PDF in Fig. 5. In the O$_3$ PDFs the normalised mixing entropy values enlarge with an increase in the coordinate value, i.e. height. Below PV values of $\approx$2 PVU the normalised mixing entropy is considerably small, indicating only small-scale and low trace gas variability. A low mixing entropy value indicates a rather homogeneous air mass. This seems counterintuitive, since a well-mixed state, as an equilibrium state, should have maximum entropy. It should be noted that SE is distinct from the thermodynamical entropy. Thus, the entropy here is considered in the "chemical space" in contrast to the "physical space" (Sparling, 2000). The PDFs show highest entropy values in the LMS for O$_3$ and in the troposphere as well as in the extra-tropical transition layer for H$_2$O. The corresponding trace gas variability is maximal in these regions, implying the occurrence of different mixing states.

In all used different coordinates, normalised mixing entropy values show a reversed course for O$_3$ and H$_2$O (for mixing entropies related to Θ, $\triangle\Theta_2$ and $\triangle\Theta_4$ see Krebsbach, 2005). Total water VMRs are highly variable in the troposphere, whereas ozone is comparably homogeneously distributed with respect to the bin size of the considered coordinate. Due to the strong gradient of both trace gases at or in the vicinity of the tropopause, normalised mixing entropy values ($SE/SE_{\max}$) increase for O$_3$ and decrease for H$_2$O with further penetration into the LMS. Therefore, at a PV value of $\approx$2 PVU also stronger gradients in the course of normalised mixing entropies are evident for almost all seasons. The spread of trace gas VMRs in different bins of the reference coordinate is reflected in the value for $SE/SE_{\max}$. Owing to the tropopause crossings of the aircraft (at least 16 times each season) and the first flight leg near the tropopause region, there is a large amount of data in the vicinity of the tropopause, reducing data gaps with respect to the chosen bin widths. This holds at least for O$_3$, and, due to the strong gradient of H$_2$O in that region with VMR variations covering 2–

Table 1. Pearson's r (left) and Spearman's rank ϱ (right) correlation coefficients for O_3 (top) and H_2O (bottom) versus potential temperature (Θ), potential vorticity (PV), distance to the local dynamically defined tropopause (i.e. 2, 3, 4 PVU surface, $\triangle\Theta_2$, $\triangle\Theta_3$, $\triangle\Theta_4$, respectively), and pressure (p). The coefficients of the eight single SPURT campaigns (IOP 1–8) are given for the two campaigns in each season, as indicated by the corresponding month and year (mm/yy). Best correlation coefficients (negative or positive) are highlighted in bold.

IOPs: mm/yy	functional correlation Pearson r: O_3 vs.						structural correlation Spearman ϱ: O_3 vs.					
	Θ	PV	$\triangle\Theta_2$	$\triangle\Theta_3$	$\triangle\Theta_4$	p	Θ	PV	$\triangle\Theta_2$	$\triangle\Theta_3$	$\triangle\Theta_4$	p
1, 5: 11/01, 10/02	0.58	**0.87**	0.85	0.85	0.85	−0.29	0.59	0.90	0.89	0.90	**0.90**	−0.23
2, 6: 01/02, 02/03	0.80	0.86	0.91	**0.92**	0.91	−0.49	0.82	0.91	0.93	**0.94**	0.93	−0.55
3, 7: 05/02, 04/03	0.82	0.91	**0.93**	0.93	0.92	−0.50	0.84	0.92	**0.94**	0.94	0.93	−0.48
4, 8: 08/02, 07/03	0.47	**0.84**	0.76	0.78	0.80	−0.27	0.47	**0.89**	0.80	0.84	0.87	−0.25
	Pearson r: H_2O vs.						Spearman ϱ: H_2O vs.					
	Θ	PV	$\triangle\Theta_2$	$\triangle\Theta_3$	$\triangle\Theta_4$	p	Θ	PV	$\triangle\Theta_2$	$\triangle\Theta_3$	$\triangle\Theta_4$	p
1, 5: 11/01, 10/02	−0.50	−0.45	−0.43	−0.44	−0.45	**0.70**	−0.79	−0.72	**−0.82**	−0.82	−0.81	0.57
2, 6: 01/02, 02/03	−0.46	−0.49	−0.43	−0.43	−0.44	**0.70**	−0.55	**−0.60**	−0.56	−0.54	−0.54	0.60
3, 7: 05/02, 04/03	−0.46	−0.47	−0.39	−0.39	−0.39	**0.67**	**−0.67**	−0.62	−0.62	−0.61	−0.59	0.55
4, 8: 08/02, 07/03	−0.60	−0.50	−0.50	−0.47	−0.44	**0.72**	**−0.81**	−0.64	−0.75	−0.72	−0.66	0.72

3 orders of magnitude, also for H_2O above $\approx$0–1 PVU. The strong increase in SE/SE_{max} from 0–1 PVU for H_2O is due to some data gaps in the selected bin widths and the result of the strong variation in H_2O in the tropopause region with different p_is.

There are also strong gradients in SE/SE_{max} for H_2O, e.g. near 8 PVU. They result (i) from the compact relationship between the trace gas and the reference coordinate in that region (cf. PDFs) and/or (ii) from a bimodal distribution above $\approx$8 PVU, both decreasing SE/SE_{max}. During spring the O_3 variability is highest in the LMS, probably due to the enhanced downward motion. The O_3 entropy values are hence maximal during this season. The same arises for the enhanced H_2O content and its variability in the LMS during the summer months. Due to the most compact H_2O PDF for the observations in autumn, the normalised mixing entropy values result in the lowest values in the range 6–8 PVU. The seasonal trace gas cycles are therefore reflected by the seasonal course of the mixing entropies.

Despite the comprehensive data coverage in the UT/LMS obtained during the SPURT project, it should be mentioned that to derive a more valuable statement from the mixing entropy, considerably more measurements are required, in particular in the upper LMS.

4.3 Functional and structural correlations

A common measure for a relation between ordinal or continuous variables is the product-moment coefficient. Pearson's correlation coefficient (r) reflects the degree of linear relationship between two variables, say x and y, of dimension

N. The functional correlation is defined as

$$r_{xy} = \frac{\sum_{i=1}^{N}(x_i - \bar{x})(y_i - \bar{y})}{\sqrt{\sum_{i=1}^{N}(x_i - \bar{x})^2}\sqrt{\sum_{i=1}^{N}(y_i - \bar{y})^2}}, \qquad (3)$$

with $\bar{x}$ ($\bar{y}$) as the mean of the x_i's (y_i's). It can range from −1 to +1, inclusive, i.e. from a perfect negative to a perfect positive correlation, whereby $r=0$ indicates that x and y are uncorrelated. To decide, whether a correlation is significantly stronger than another, Pearson's r is not an accurate measure, since the individual distributions of x and y are not considered.

A more structural measure for the relationship between two variables provides Spearman's correlation coefficient (ϱ), which is a non-parametric or rank correlation. The computation is performed by replacing the value of each x_i by the value of its rank, i.e. the smallest value of variable x is converted to rank 1, the highest to rank N. The same applies for the y_i values. An outstanding advantage of the rank correlation is that a non-parametric correlation is more robust than a linear correlation, in the same sense as the median is more robust than the mean (Press et al., 1997). After converting the numbers to ranks the Spearman correlation coefficient is calculated according to Eq. (3).

In Table 1 both Pearson's and Spearman's correlation coefficients are shown for O_3 (top) versus different parameters. Ozone does not show best correlations with potential temperature. As is directly evident from both coefficients, highest positive correlations appear when O_3 is related to PV and/or to $\triangle\Theta$. The coefficients are also high for almost all chosen PV threshold values to define the local dynamical tropopause. Further, this rather simple measure for the

association between two parameters reveal the conclusion drawn from the PDFs. Trace gas isopleths of O$_3$ seem to be orientated along surfaces of PV rather than along isentropes. The differences between r and ϱ for PV and the $\triangle \Theta$s are only small. In contrast, the correlations of O$_3$ with pressure are comparatively insignificant, nevertheless exhibiting larger structural negative coefficients during some winter and spring campaigns.

The correlation coefficients for H$_2$O versus different parameters are listed in Table 1 (bottom). When calculating Pearson's r, H$_2$O is best correlated with pressure. Both, p and H$_2$O, decrease very rapidly with height in a rather logarithmic manner. Thus, the good correlation is to be expected. This is especially evident during the summer campaigns (IOP 4 and IOP 8). Spearman's ϱ is independent on the mode or shape of the distribution, and it renders unnecessary to make assumptions on the functional relationship (Press et al., 1997). For this measure, H$_2$O shows, as O$_3$, a high degree of correlation when related to Θ, $\triangle \Theta$ and PV.

5 Conclusions

The unique, continuous and high resolution O$_3$ and H$_2$O measurements, obtained during the SPURT campaigns between November 2001 and July 2003, allow for a comprehensive view of the UT/LMS region above Europe. In the first part, seasonal cycles of O$_3$ and H$_2$O in the UT and LMS have been analysed. As indicated by extensive studies of vertical profiles obtained during ascents and descents (see Hoor et al., 2004; Krebsbach, 2005), the tropopause location, i.e. the noticeable boundary between the troposphere and the stratosphere, coincides well with the 2 PVU surface. Different analyses of the trace gas measurements reveal that the seasonal cycle of O$_3$ in the UT shows a spring to summer maximum, most probably affected by in situ photochemistry (cf. also Hegglin et al., 2005). In the LMS the seasonal O$_3$ cycle is more pronounced and shifted in phase by about 2–3 months earlier in the year, exhibiting a distinct spring time maximum. In the upper part of the LMS, a pronounced O$_3$ maximum is established during spring, whereas the lower part of the LMS still contains large contributions of rather O$_3$-poor tropospheric air during winter and early spring. Only around April (2003) the O$_3$ maximum is also established in the lower part. This is the effect of the large-scale stratospheric winter/spring Brewer-Dobson circulation (see also Hegglin et al., 2005; Krebsbach et al., 2006). Induced by breaking Rossby waves and strong diabatic subsidence (the downward control principle, Haynes et al., 1991) aged and O$_3$-rich stratospheric air is transported downward into the LMS (e.g. Austin and Follows, 1991; Beekmann et al., 1994; Logan, 1999). Thus, during spring a contribution of stratospheric O$_3$ due to stratosphere-to-troposphere transport is likely to affect tropospheric O$_3$.

In contrast to the O$_3$ seasonal cycles, H$_2$O shows no phase shift between the UT and the LMS. In a seasonal view, maximum H$_2$O VMRs were observed during the summer campaigns close to the tropopause in the UT as well as in the LMS. Lowest H$_2$O VMRs were measured during the winter and autumn deployments, the latter indicating a temporally link with the subtropics/tropics (cf. Hoor et al., 2005, Hegglin et al., 2005, Krebsbach et al., 2006b[2]). The reason for this seasonality is twofold. First, since H$_2$O is strongly influenced by heterogeneous processes, it follows the temperature variation at the tropopause, i.e. the air is widely freeze-dried during its transport into the LMS (see also Krebsbach et al., 2006b). Second, whereas downward transport of dry air from the overworld into the LMS is dominant during winter, the barrier for quasi-isentropic transport of moist air over the tropopause deep into the LMS is weaker during summer.

To examine the distribution, spread, and variability of both trace gases, especially 2-dimensional probability distributions were used. Moreover, from these distributions, effects of transport and mixing processes can be inferred. Considering several chemical, thermal, and dynamical coordinates, the measured trace gases are most compact arranged and best correlated when related to potential vorticity and to distance to the dynamically defined tropopause. Using various PV threshold values for the extra-tropical tropopause, the distributions show almost the same shape. The trace gas isopleths follow surfaces of PV or the shape of the tropopause, in accordance with results from Hoor et al. (2004). This suggests an advanced mixing state in the LMS on surfaces relative to the shape of the tropopause.

The mixing entropy is assigned to characterise the PDFs and to estimate trace gas variability. Mixing entropy values for O$_3$ and H$_2$O in the LMS appear to be maximal during spring and summer, respectively. This indicates highest variability of these trace gases during the respective seasons with greater impact of stratospheric air during spring and tropospheric air during summer. Notwithstanding the extensive SPURT data set, still more data are necessary to derive more robust statements from the mixing entropy.

Despite the large seasonal and spatial data coverage, SPURT alone can obviously not provide a climatology but it reduces the lack of measurements in the UT/LMS, in particular above Europe. The SPURT measurements can only provide instantaneous representations of the atmosphere encountered during the single flights. To derive annual trace gas cycles, SPURT data from different years are assembled which are likely affected by inter-annual variability and/or by sampling. It must thus be emphasised that the results presented here only apply for the SPURT region and have to be confirmed by further investigations and measurements.

---

[2]Krebsbach, M., Schiller, C., Günther, G., and Wernli, H.: Transport across the extra-tropical tropopause and impact on the H$_2$O content of the LMS, in preparation, 2006b.

Table A1. Number of seasonal data points in each considered Θ bin in Fig. 4.

Θ bin in K	O$_3$				H$_2$O			
	aut	win	spr	sum	aut	win	spr	sum
280	19	–	–	–	–	–	–	–
285	13	–	–	–	1	–	–	–
290	43	28	–	–	112	60	1	–
295	67	53	12	–	51	141	25	–
300	117	98	42	–	62	315	101	–
305	340	411	230	–	259	669	295	1
310	259	556	602	–	296	1036	639	32
315	387	936	389	117	488	1045	533	142
320	941	1999	1715	437	929	2115	1951	528
325	1009	2229	1916	773	1031	2277	2095	596
330	1753	2427	2721	1196	1580	2459	2721	588
335	1945	2131	2498	3165	1780	2176	2498	2657
340	1721	2296	3439	2651	1720	2377	3439	2046
345	2683	2628	2697	1935	2681	2667	2697	1341
350	2423	2729	2191	2224	2423	2590	2191	1232
355	2455	3030	2369	3832	2454	2555	2369	3553
360	2904	1422	1955	2479	2899	1281	1951	2186
365	849	366	2055	586	849	366	2055	410
370	150	222	608	171	150	222	606	99
375	–	–	110	–	–	–	110	–

Table A2. Number of seasonal data points in each considered PV bin in Fig. 5.

PV bin in PVU	O$_3$				H$_2$O			
	aut	win	spr	sum	aut	win	spr	sum
0.0	327	855	544	198	348	1299	996	432
0.5	996	820	476	561	1049	956	739	785
1.0	1307	746	930	495	1420	961	927	408
1.5	1186	1187	975	823	1165	1298	988	730
2.0	643	1228	1559	844	652	1340	1563	488
2.5	389	595	1387	1371	487	658	1387	1205
3.0	703	620	832	862	690	703	832	684
3.5	573	683	1268	1399	558	741	1268	1177
4.0	467	512	1316	1180	449	562	1316	880
4.5	408	940	2019	1202	385	879	2019	963
5.0	428	1676	745	1277	416	1293	744	982
5.5	730	1362	1189	1087	694	1288	1189	800
6.0	954	1831	1587	1747	927	1827	1587	1437
6.5	1970	2587	1819	1049	1873	2604	1819	734
7.0	2119	3872	2416	1393	1858	3993	2416	833
7.5	2245	1628	2069	1454	2184	1533	2068	1089
8.0	1503	1510	2805	1920	1503	1508	2801	1378
8.5	1200	653	838	410	1200	653	838	217
9.0	871	183	446	251	871	183	446	173
9.5	225	70	214	42	223	70	214	16
10.0	426	–	110	–	423	–	110	–
10.5	378	–	–	–	378	–	–	–

Table A3. Number of seasonal data points in each considered $\triangle\Theta_2$ bin in Fig. 6.

$\triangle\Theta_2$ bin in K	O$_3$				H$_2$O			
	aut	win	spr	sum	aut	win	spr	sum
−45	3	–	–	–	–	–	–	–
−40	12	5	–	–	–	–	–	–
−35	14	23	–	–	–	–	–	19
−30	14	35	–	66	26	–	2	78
−25	78	79	–	66	54	75	61	105
−20	162	155	26	131	173	208	152	194
−15	840	355	396	168	819	655	590	316
−10	825	1188	714	544	949	1483	996	669
−5	1969	1769	2077	1200	2059	2081	2138	1037
0	800	1767	2797	2218	845	1921	2800	1613
5	1023	1432	2278	1737	1027	1602	2278	1051
10	884	1220	3064	3713	837	1310	3064	3211
15	736	1185	1451	2260	695	1139	1451	1858
20	1188	2423	2391	2073	1091	1955	2391	1503
25	1968	1620	1973	1633	1715	1626	1972	967
30	1440	2142	796	1911	1377	2167	796	1475
35	1314	1165	1522	931	1313	1234	1522	811
40	839	1960	1997	241	839	1972	1994	179
45	1086	1391	968	164	1085	1334	968	80
50	1869	1014	772	151	1867	957	772	92
55	1214	1337	505	272	1212	1337	505	67
60	893	1044	636	86	893	1044	635	86
65	719	239	476	–	719	239	475	–
70	158	10	259	–	158	10	259	–
75	–	–	384	–	–	–	384	–

Appendix: Number of data points considered in the PDFs

To provide an additional information for the robustness of the PDFs (Figs. 4–6), the number of data points considered in each bin of the reference coordinate are shown seasonally separated in Tables A1–A3.

References

Ancellet, G. and Beekmann, M.: Evidence for changes in the ozone concentrations in the free troposphere over southern France from 1976 to 1995, Atmos. Environ., 31, 2835–2851, 1997.

Appenzeller, C., Holton, J. H., and Rosenlof, K. H.: Seasonal variation of mass transport across the tropopause, J. Geophys. Res., 101, 15 071–15 078, 1996.

Austin, J. F. and Follows, M. J.: The ozone record at Payerne: An assessment of the cross-tropopause flux, Atmos. Environ., 25, 1873–1880, 1991.

Especially, the observed high amounts of H$_2$O accompanied with stratospheric O$_3$ VMRs need further investigations and supporting model studies. Analyses of Arctic measurements near the northern SPURT area by Pfister et al. (2003) show no such occurrences. In contrast, these conditions have been encountered several times during SPURT, both on southbound and northbound flights, and it is not clear if these appearances can be attributed to climate trend or to geographical conditions, e.g. wave breaking zone.

Beekmann, M., Ancellet, G., and Mégie, G.: Climatology of tropospheric ozone in southern Europe and its relation to potential vorticity, J. Geophys. Res., 99, 12 841–12 853, 1994.

Brennikmeijer, C. A. M., Slemr, F., Koeppel, C., Scharffe, D. S., Pupek, M., Lelieveld, J., Crutzen, P., Zahn, A., Sprung, D., Fischer, H., Hermann, M., Reichelt, M., Heintzenberg, J., Schlager, H., Ziereis, H., Schumann, U., Dix, B., Platt, U., Ebinghaus, R., Martinsson, B., Ciais, P., Filippi, D., Leuenberger, M., Oram, D., Penkett, S., van Velthoven, P., and Waibel, A.: Analyzing Atmospheric Trace Gases and Aerosols Using Passenger Aircraft, EOS, 86, 2005.

Brunner, D., Staehelin, J., and Jeker, D.: Large-Scale Nitrogen Oxide Plumes in the Tropopause Region and Implications for Ozone, Science, 282, 1305–1309, 1998.

Brunner, D., Staehelin, J., Jeker, D., Wernli, H., and Schumann, U.: Nitrogen oxides and ozone in the tropopause region of the Northern Hemisphere: Measurements from commercial aircraft in 1995/1996 and 1997, J. Geophys. Res., 106, 27 673–27 699, 2001.

Chen, P.: Isentropic cross-tropopause mass exchange in the extratropics, J. Geophys. Res., 100, 16 661–16 673, 1995.

Derwent, R. G., Simmonds, P. G., Seuring, S., and Dimmer, C.: Observation and interpretation of the seasonal cycles in the surface concentrations of ozone and carbon monoxide at Mace Head, Ireland from 1990 to 1994, Atmos. Environ., 32, 145–157, 1998.

Dessler, A. E. and Sherwood, S. C.: Effect of convection on the summertime extratropical lower stratosphere, J. Geophys. Res., 109, D23301, doi:10.1029/2004JD005209, 2004.

Dessler, A. E., Hintsa, E. J., Weinstock, E. M., Anderson, J. G., and Chan, K. R.: Mechanisms controlling water vapor in the lower stratosphere: "A tale of two stratospheres", J. Geophys. Res., 100, 23 167–23 172, 1995.

Eluszkiewicz, J.: A three-dimensional view of the stratosphere-to-troposphere exchange in the GFDL SKYHI model, Geophys. Res. Lett., 23, 2489–2492, 1996.

Engel, A., Bönisch, H., Brunner, D., Fischer, H., Franke, H., Günther, G., Gurk, C., Hegglin, M., Hoor, P., Königstedt, R., Krebsbach, M., Maser, R., Parchatka, U., Peter, T., Schell, D., Schiller, C., Schmidt, U., Spelten, N., Szabo, T., Weers, U., Wernli, H., Wetter, T., and Wirth, V.: Highly resolved observations of trace gases in the lowermost stratosphere and upper troposphere from the SPURT project: an overview, Atmos. Chem. Phys. Discuss., 5, 5081–5126, 2005,
SRef-ID: 1680-7375/acpd/2005-5-5081.

Foot, J. S.: Aircraft measurements of the humidity in the lower stratosphere from 1977 to 1980 between 45° N and 65° N, Quart. J. Roy. Meteor. Soc., 110, 303–319, 1984.

Good, P. and Pyle, J.: Refinements in the use of equivalent latitude for assimilating sporadic inhomogeneous stratospheric tracer observations, 1: Detecting transport of Pinatubo aerosol across a strong vortex edge, Atmos. Chem. Phys., 4, 1823–1836, 2004,
SRef-ID: 1680-7324/acp/2004-4-1823.

Günther, G., Schiller, C., Konopka, P., and Krebsbach, M.: Simulation of Transport Processes in the Tropopause Region during SPURT using a Lagrangian Model, Geophys. Res. Abstr., 6, 02609, 2004.

Haynes, P. and Shepherd, T.: Report on the SPARC Tropopause Workshop, Bad Tölz, Germany, 17–21 April 2001, SPARC newsletter N. 17, 2000.

Haynes, P. H., Marks, C. J., McIntyre, M. E., Sheperd, T. G., and Shine, K. P.: On the "downward control" of extratropical diabatic circulations by eddy-induced mean zonal forces, J. Atmos. Sci., 48, 651–678, 1991.

Hegglin, M. I.: Airborne NO_y-, NO- and O_3-measurements during SPURT: Implications for atmospheric transport, Ph.D. thesis, Swiss Federal Institute of Technology Zürich, Diss. ETH No. 15553, 2004.

Hegglin, M. I., Brunner, D., Wernli, H., Schwierz, C., Martius, O., Hoor, P., Fischer, H., Parchatka, U., Spelten, N., Schiller, C., Krebsbach, M., , Weers, U., Staehelin, J., and Peter, Th.: Tracing troposphere-to-stratosphere transport above a mid-latitude deep convective system, Atmos. Chem. Phys., 4, 741–756, 2004,
SRef-ID: 1680-7324/acp/2004-4-741.

Hegglin, M. I., Brunner, D., Peter, Th., Hoor, P., Fischer, H., Staehelin, J., Krebsbach, M., Schiller, C., Parchatka, U., and Weers, U.: Measurements of NO, NO_y, N_2O, and O_3 during SPURT: implications for transport and chemistry in the lowermost stratosphere, Atmos. Chem. Phys. Discuss., 5, 8649–8688, 2005,
SRef-ID: 1680-7375/acpd/2005-5-8649.

Hintsa, E. J., Weinstock, E. M., Dessler, A. E., Anderson, J. G., Loewenstein, M., and Podolske, J. R.: SPADE H_2O measurements and the seasonal cycle of stratospheric water vapor, Geophys. Res. Lett., 21, 2559–2562, 1994.

Hintsa, E. J., Boering, K. A., Weinstock, E. M., Anderson, J. G., Gary, B. L., Pfister, L., Daube, B. C., Wofsy, S. C., Loewenstein, M., Podolske, J. R., Margitan, J. J., and Bui, T. P.: Troposhere-to-stratosphere transport in the lowermost stratosphere from measurements of H_2O, CO_2, N_2O and O_3, Geophys. Res. Lett., 25, 2655–2658, 1998.

Hoinka, K. P.: Temperature, Humidity, and Wind at the Global Tropopause, Mon. Wea. Rev., 127, 2248–2265, 1999.

Hollingsworth, A. and Lönneberg, P.: The verification of objective analyses: Diagnostics of analysis system performance, Met. Atmos. Phys., 40, 3–27, 1989.

Holton, J. R., Haynes, P. H., McIntyre, M. E., Douglass, A. R., Rood, R. B., and Pfister, L.: Stratosphere-troposphere exchange, Rev. Geophys., 33, 403–439, 1995.

Hoor, P., Gurk, C., Brunner, D., Hegglin, M. I., Wernli, H., and Fischer, H.: Seasonality and extent of extratropical TST derived from in-situ CO measurements during SPURT, Atmos. Chem. Phys., 4, 1427–1442, 2004,
SRef-ID: 1680-7324/acp/2004-4-1427.

Hoor, P., Fischer, H., and Lelieveld, J.: Tropical and extratropical tropospheric air in the lowermost stratosphere over Europe: A CO-based budget, Geophys. Res. Lett., 32, L07802, doi:10.1029/2004GL022018, 2005.

Hoskins, B. J.: Towards a $PV - \theta$ view of the general circulation, Tellus, 43AB, 27–35, 1991.

Hoskins, B. J., McIntyre, M. E., and Robertson, A. W.: On the use and significance of isentropic potential vorticity maps, Quart. J. Roy. Meteor. Soc., 111, 877–946, 1985.

Hough, A. M.: Development of a two-dimensional global tropospheric model: Model chemistry, J. Geophys. Res., 96, 7325–7362, 1991.

Inamdar, A. K. and Ramanathan, V.: Tropical and global scale interactions among water vapor, atmospheric greenhouse effect, and surface temperature, J. Geophys. Res., 103, 32 177–32 194, 1998.

Krebsbach, M.: Trace gas transport in the UT/LS: seasonality, stratosphere-troposphere exchange and implications for the extra-tropical mixing layer derived from airborne O_3 and H_2O measurements, Ph.D. thesis, Bergische Universität Wuppertal, http://nbn-resolving.de, urn:nbn:de:hbz:468-20050180, 2005.

Lindzen, R. S.: Some Coolness Concerning Global Warming, Bull. Am. Met. Soc., 71, 288–299, 1990.

Liu, S. C., Trainer, M., Fehsenfeld, F., Parrish, D., Williams, E. J., Fahey, D. W., Hübler, G., and Murphy, P. C.: Ozone production in the rural troposphere and the implications for regional and global ozone distributions, J. Geophys. Res., 92, 4191–4207, 1987.

Logan, J.: Tropospheric ozone: Seasonal behaviour, trends and anthropogenic influence, J. Geophys. Res., 90, 10 463–10 482, 1985.

Logan, J.: Ozone in rural areas of the United States, J. Geophys. Res., 94, 8511–8532, 1989.

Logan, J. A.: An analysis of ozonesonde data for the lower stratosphere: Recommendations for testing models, J. Geophys. Res., 104, 16 151–16 170, 1999.

Marenco, A., Válerie, T., Nédélec, P., Smit, H., Helten, M., Kley, D., Karcher, F., Simon, P., Law, K., Pyle, J., Poschmann, G., von Wrede, R., Hume, C., and Cook, T.: Measurement of ozone and water vapor by Airbus in-service aircraft: The MOZAIC airborne program, An overview, J. Geophys. Res., 103, 25 631–25 642, 1998.

Mastenbrook, H. J. and Oltmans, H. J.: Stratospheric Water Vapor Variability for Washington, DC/Boulder, CO: 1964–82, J. Atmos. Sci., 40, 2157–2165, 1983.

McLinden, C. A., Olsen, S. C., Hannegan, B., Wild, O., Prather, M. J., and Sundet, J.: Stratospheric ozone in 3-D models: A simple chemistry and the cross-tropopause flux, J. Geophys. Res., 105, 14 653–14 665, 2000.

Monks, P. S.: A review of the observations and origins of the spring ozone maximum, Atmos. Environ., 34, 3545–3561, 2000.

Mottaghy, D.: Ozonmessungen in der unteren Stratosphäre, Master's thesis, Rheinisch-Westfälische Technische Hochschule Aachen, in cooperation with the Institute for Chemistry and Dynamics of the Geosphere, ICG-I: Stratosphere, 2001.

Nedoluha, G. E., Bevilacqua, R. M., Hoppel, K. W., Lumpe, J. D., and Smit, H.: Polar Ozone and Aerosol Measurement III measurements of water vapor in the upper troposphere and lowermost stratosphere, J. Geophys. Res., 107, 4103, doi:10.1029/2001JD000793, 2002.

Oltmans, S. J. and Hofmann, D. J.: Increase in lower-stratospheric water vapour at a mid-latitude Northern Hemisphere site from 1981 to 1994, Nature, 374, 146–149, 1995.

Oltmans, S. J. and Levy II, H.: Surface ozone measurements from a global network, Atmos. Environ., 28, 9–24, 1994.

Pan, L., Solomon, S., Randel, W., Lamarque, J.-F., Hess, P., Gille, J., Chiou, E.-W., and McCormick, M. P.: Hemispheric asymmetries and seasonal variations of the lowermost stratospheric water vapor and ozone derived from SAGE II data, J. Geophys. Res., 102, 28 177–28 184, 1997.

Pan, L. L., Hintsa, E. J., Stone, E. M., Weinstock, E. M., and Randel, W. J.: The seasonal cycle of water vapor and saturation vapor mixing ratio in the extratropical lowermost stratosphere, J. Geophys. Res., 105, 26 519–26 530, 2000.

Park, M., Randel, W. J., Kinnison, D. E., and Gracia, R. R.: Sea-

sonal variation of methane, water vapor, and nitrogen oxides near the tropopause: Satellite observations and model simulations, J. Geophys. Res., 109, D03302, doi:10.1029/2003JD003706, 2004.

Pfister, L., Selkirk, H. B., Jensen, E. J., Podolske, J., Sachse, G., Avery, M., Schoeberl, M. R., Mahoney, M. J., and Richard, E.: Processes controlling water vapor in the winter Arctic tropopause region, J. Geophys. Res., 108, 8314, doi:10.1029/2001JD001067, 2003.

Prados, A. I., Nedoluha, G. E., Bevilacqua, R. M., Allen, D. R., Hoppel, K. W., and Marenco, A.: POAM III ozone in the upper troposphere and lowermost stratosphere: Seasonal variability and comparisons to aircraft observations, J. Geophys. Res., 108, 4218, doi:10.1029/2002JD002819, 2003.

Press, W. H., Teukolsky, S. A., Vetterling, W. T., and Flannery, B. P.: Numerical Recipies in Fortran 77: The Art of Scientific Computing, vol. 1 of "Fortran Numerical Recipies", Press Syndicate of the University of Cambridge, The Pitt Building, Trumpington Street, Cambridge CB2 1RP, 2nd edn., ISBN 0-521-43064-X, 1997.

Randel, W. J., Wu, F., Gettelman, A., Russell III, J. M., Zawodny, J. M., and Oltmans, S. J.: Seasonal variation of water vapor in the lower stratosphere observed in Halogen Occultation Experiment data, J. Geophys. Res., 106, 14 313–14 325, 2001.

Ray, E. A., Moore, F. L., Elkins, J. W., Dutton, G. S., Fahey, D. W., Vömel, H., Oltmans, S. J., and Rosenlof, K. H.: Transport into the Northern Hemisphere lowermost stratosphere revealed by in situ tracer measurements, J. Geophys. Res., 104, 26 565–26 580, 1999.

Ray, E. A., Rosenlof, K. H., Richard, E., Parrish, D., and Jakoubek, R.: Distributions of ozone in the region of the subtropical jet: An analysis of in situ aircraft measurements, J. Geophys. Res., 109, D08106, doi:10.1029/2003JD004143, 2004a.

Ray, E. A., Rosenlof, K. H., Richard, E. C., Hudson, P. K., Cziczo, D. J., Loewenstein, M., Jost, H.-J., Lopez, J., Ridley, B., Weinheimer, A., Montzka, D., Knapp, D., Wofsy, S. C., Daube, B. C., Gerbig, C., Xueref, I., and Herman, R. L.: Evidence of the effect of summertime midlatitude convection on the subtropical lower stratosphere from CRYSTAL-FACE tracer measurements, J. Geophys. Res., 109, D18304, doi:10.1029/2004JD004655, 2004b.

Rind, D., Chiou, E.-W., Chu, W., Larsen, J., Oltmans, S., Lerner, J., McCormick, M. P., and McMaster, L.: Positive water vapour feedback in climate models confirmed by satellite data, Nature, 349, 500–502, 1991.

Scheel, H. E., Areskoug, H., Geiß, H., Gomiscek, B., Granby, K., Haszpra, L., Klasinc, L., Kley, D., Laurila, T., Lindskog, A., Roemer, M., Schmitt, R., Simmonds, P., Solberg, S., and Toupance, G.: On the Spatial Distribution and Seasonal Variation of Lower-Troposphere Ozone over Europe, J. Atmos. Chem., 28, 11–28, 1997.

Schmitt, R. and Volz-Thomas, A.: Climatology of Ozone, PAN, CO, and NMHC in the Free Troposphere Over the Southern North Atlantic, J. Atmos. Chem., 28, 245–262, 1997.

Sparling, L. C.: Statistical perspectives on stratospheric transport, Rev. Geophys., 38, 417–436, 2000.

Sparling, L. C. and Schoeberl, M. R.: Mixing entropy analysis of dispersal of aircraft emissions in the lower stratosphere, J. Geophys. Res., 100, 16 805–16 812, 1995.

Sprenger, M. and Wernli, H.: A northern hemispheric climatology

of cross-tropopause exchange for the ERA15 time period (1979–1993), J. Geophys. Res., 108, 8521, doi:10.1029/2002JD002636, 2003.

Srikanth, M., Kesavan, H. K., and Roe, P. H.: Probability Density Function Estimation using the MinMax Measure, IEEE Transactions on Systems, Man, and Cybernetics – Part C: Applications and Reviews, 30, 77–83, 2000.

Stone, E. M., Pan, L., Sandor, B. J., Read, W. G., and Waters, J. W.: Spatial distributions of upper tropospheric water vapor measurements from the UARS Microwave Limb Sounder, J. Geophys. Res., 105, 12 149–12 161, 2000.

Strahan, S. E.: Climatologies of lower stratospheric NO_y and O_3 and correlations with N_2O based on in situ observations, J. Geophys. Res., 104, 30 463–30 480, 1999.

Tuck, A. F., Hovde, S. J., Kelly, K. K., Mahoney, M. J., Proffitt, M. H., Richard, E. C., and Thompson, T. L.: Exchange between the upper tropical troposphere and the lower stratosphere studied with aircraft observations, J. Geophys. Res., 108, D23, 4734, 2003.

Wang, P.-H., Cunnold, D. M., Zawodny, J. M., Pierce, R. B., Olson, J. R., Kent, G. S., and Skeens, K. M.: Seasonal ozone variations in the isentropic layer between 330 and 380 K as observed by SAGE II: Implications of extratropical cross-tropopause transport, J. Geophys. Res., 103, 28 647–28 659, 1998.

WMO: Atmospheric Ozone 1985, WMO Global Ozone Res. and Monit. Proj. Rep. 20, Geneva, 1986.

Zahn, A., Brenninkmeijer, C. A. M., and van Velthoven, P. F. J.: Passenger aircraft project CARIBIC 1997–2002, Part II: the ventilation of the lowermost stratosphere, Atmos. Chem. Phys. Discuss., 4, 1119–1150, 2004,
SRef-ID: 1680-7375/acpd/2004-4-1119.

Zöger, M., Afchine, A., Eicke, N., Gerhards, M.-T., Klein, E., McKenna, D. S., Mörschel, U., Schmidt, U., Tan, V., Tuitjer, F., Woyke, T., and Schiller, C.: Fast in situ stratospheric hygrometers: A new family of balloon-borne and airborne Lyman α photofragment fluorescence hygrometers, J. Geophys. Res., 104, 1807–1816, 1999.